Hurricane Sally (2020) Shifts the Ocean Thermal Structure across the Inner Core during Rapid Intensification over the Shelf

B. DZWONKOWSKI,[a,b] S. FOURNIER,[c] G. LOCKRIDGE,[b] J. COOGAN,[d] Z. LIU,[a] AND K. PARK[e]

[a] *University of South Alabama, Mobile, Alabama*
[b] *Dauphin Island Sea Lab, Dauphin Island, Alabama*
[c] *Jet Propulsion Laboratory, California Institute of Technology, Pasadena, California*
[d] *Woods Hole Oceanographic Institution, Woods Hole, Massachusetts*
[e] *Texas A&M University at Galveston, Galveston, Texas*

(Manuscript received 18 January 2022, in final form 12 July 2022)

ABSTRACT: Prediction of rapid intensification in tropical cyclones prior to landfall is a major societal issue. While air–sea interactions are clearly linked to storm intensity, the connections between the underlying thermal conditions over continental shelves and rapid intensification are limited. Here, an exceptional set of in situ and satellite data are used to identify spatial heterogeneity in sea surface temperatures across the inner core of Hurricane Sally (2020), a storm that rapidly intensified over the shelf. A leftward shift in the region of maximum cooling was observed as the hurricane transited from the open gulf to the shelf. This shift was generated, in part, by the surface heat flux in conjunction with the along- and across-shelf transport of heat from storm-generated coastal circulation. The spatial differences in the sea surface temperatures were large enough to potentially influence rapid intensification processes suggesting that coastal thermal features need to be accounted for to improve storm forecasting as well as to better understand how climate change will modify interactions between tropical cyclones and the coastal ocean.

SIGNIFICANCE STATEMENT: The connections between the underlying thermal energy in the ocean that powers tropical cyclones and rapid intensification of storms over continental shelves are limited. An exceptional set of data collected in the field as well as from space with satellites was used to identify spatial variations in sea surface temperatures across the inner core of Hurricane Sally (2020), a storm that rapidly intensified over the shelf. The spatial differences were due to the heat loss from the surface of the ocean as well as heat transport by shelf currents. The spatial differences were large enough to potentially influence how quickly storms can intensify, suggesting that coastal thermal features need to be accounted for to improve storm forecasting.

KEYWORDS: Seas/gulfs/bays; Atmosphere–ocean interaction; Currents; Tropical cyclones; Buoy observations; In situ oceanic observations

1. Introduction

Exposure to hazards from tropical cyclones is a major stressor on natural and anthropogenic systems in coastal regions across the globe. The severity of hazards that accompany tropical cyclones—for example, wind speed, storm surge, and flash flooding—disproportionally increases with more intense storm events (Freeman and Warner 2001; Zhai and Jiang 2014). A key element in the formation of major storms (Saffir–Simpson categories 3–5) is rapid intensification [defined as a rate of wind increase of >35 kt (1 kt ≈ 0.51 m s^{-1}) over 24 h], with ~79% of storms undergoing this intensification process in their life cycles (Lee et al. 2016). Nonetheless, forecasting rapid intensification remains challenging (Kaplan et al. 2010; DeMaria et al. 2014).

This limitation is of particular concern given the findings of recent studies. Bhatia et al. (2019) provided evidence of an increase of intensification rates in the Atlantic Ocean basin stemming, in part, from anthropogenic forcing and Chu et al. (2020) projected a 150% increase in the major storms expected to impact the coastal ocean under a CO_2 doubling scenario. These findings suggest an increasing importance of rapid intensification for coastal storm forecasting. More directly, Emanuel (2017) found that rapid intensification prior to landfall is expected to be much more common in a warmer future climate. Such expectations are consistent with a number of recent studies that have showed that the shelf region can support significant intensification given the right conditions (e.g., Seroka et al. 2016; Potter et al. 2019; Zhang et al. 2019; Dzwonkowski et al. 2020; Cheriton et al. 2021). In fact, Pun et al. (2019) found that nearshore waters <30 m deep likely played a critical role in the rapid intensification of Typhoon Hato (2017) prior to landfall.

Consequently, understanding the shelf conditions and complex feedbacks that favor rapid intensification is of critical importance to coastal communities. The fortuitous path of Hurricane Sally (2020), which bisected four monitoring stations in the Mississippi

Denotes content that is immediately available upon publication as open access.

Supplemental information related to this paper is available at the Journals Online website: https://doi.org/10.1175/JPO-D-22-0025.s1.

Corresponding author: Brian Dzwonkowski, briandz@disl.org

DOI: 10.1175/JPO-D-22-0025.1

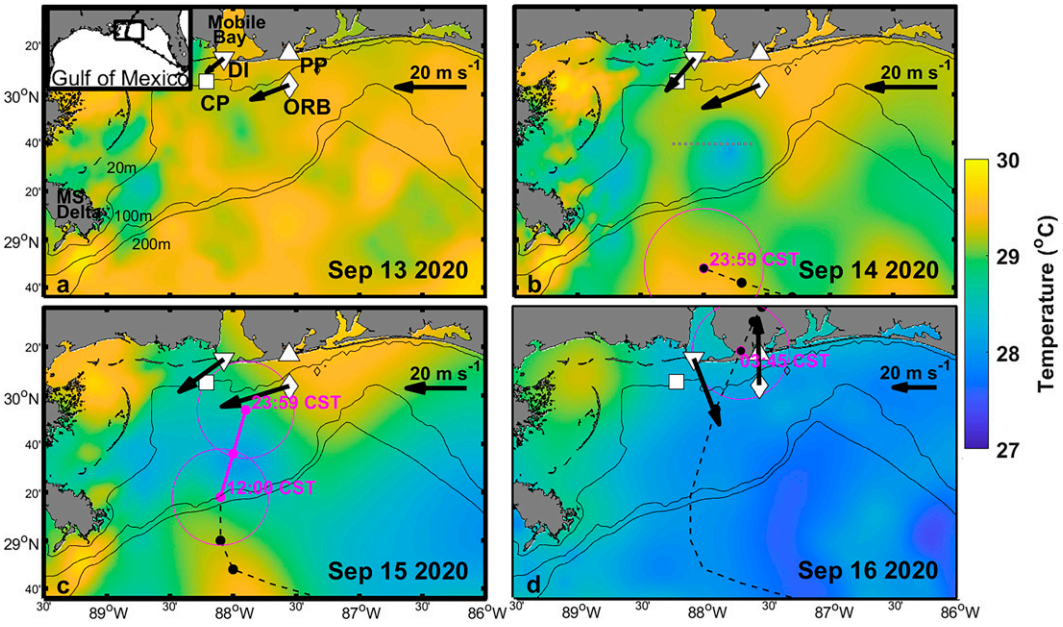

FIG. 1. A map of the Mississippi Bight showing the evolution of the sea surface temperature and coastal wind conditions (black arrows) during the transit of Hurricane Sally (2020) on (a) 13 Sep (prior to the storm arrival) and (b)–(d) 14–16 Sep. The monitoring stations, including Dauphin Island (DI; upside-down triangle), Orange Beach (ORB; diamond), FOCAL/CP (CP; square), and Perdido Pass (PP; triangle), as well as the locations of the Mississippi (MS) River Delta and Mobile Bay are shown in (a), with the inset showing the study region in the context of the broader Gulf of Mexico and the full track of Hurricane Sally. Hydrographic data were available at all four stations, whereas meteorological data were only available at DI and ORB. Thin black lines indicate selected isobaths that show the approximate location of the shelf break (100–200 m) as well as a depth (20 m) near the shelf-monitoring stations. The track of Hurricane Sally (black dashed line) is shown in (b)–(d), with the circles indicating locations during the stated day at 6-h intervals; also shown is the radius of maximum intensity (magenta-outlined circles) at selected locations (black circles with magenta edge) and times (in magenta) as well as the period of rapid intensification over the shelf [magenta line in (c)]. On 16 Sep in (d), the approximate time and location of landfall are also provided. The wind vectors are hourly values at 1200 CST in (a)–(c) and 0300 CST in (d). Note that the winds are in oceanographic convention showing the direction to which the winds were blowing and that the velocity scale size (upper-right corner) changes in (c) and (d). In (b), the horizontal gray dashed line indicates the approximate location of the bottom front of the downwelling event determined by the advection of the 28.5°C isotherm from 9 to 14 Sep as described in Dzwonkowski et al. (2021).

Bight of the northern Gulf of Mexico (Fig. 1), provided an exceptional observational perspective of a storm system that underwent rapid intensification over the shelf. The stations were well within 100 km of the storm center, a region where enthalpy fluxes are critical to storm intensity (Miyamoto and Takemi 2010). This provided a unique perspective on the coastal ocean response to a storm event as well as evidence of the potential importance that shelf temperature heterogeneity could have on storm intensification prior to landfall. This perspective of Hurricane Sally is particularly important because the shelf behavior of this tropical cyclone was not well forecast (Berg and Reinhart 2021), representing a case study that provides critical insight for improving the understanding of processes that tropical cyclone models may not be correctly resolving (Seroka et al. 2017).

2. Materials and methods

The data sources, processing, and analysis follow similar methods as those in Dzwonkowski et al. (2018, 2020), and most of the specific details from this particular time period have been described in Dzwonkowski et al. (2021). As such, only a brief overview of the datasets is provided here with a focus on the additional data sources used in this work.

a. Tropical cyclone data

Data for Hurricane Sally were acquired from the best-track file as provided by the National Oceanic and Atmospheric Administration (NOAA) National Hurricane Center (ftp://ftp.nhc.noaa.gov/atcf/btk/). The transitional speed of Hurricane Sally was determined using the distance from the center positions and the associated 6-h intervals. The resulting speeds were interpolated to the original time step. Here, the inner core of Hurricane Sally is defined as the area within the radius of maximum wind.

To provide additional context for the best-track data, model outputs of wind (north–south and east–west components) at 10-m height were collected from the North American Mesoscale Forecast System (NAM), which is produced by National

Centers for Environmental Prediction (NCEP) and archived at the National Centers for Environmental Information (NCEI). The NAM Analysis product was used (https://www.ncei.noaa.gov/data/north-american-mesoscale-model/access/analysis/). This product has a spatial resolution of 12 km and temporal resolution of 6 h. This modeling system is commonly used in hurricane research (e.g., Garzon et al. 2018; Liu et al. 2020).

b. *In situ data and associated analysis*

To understand the atmospheric and oceanic conditions during the shelf transit of Hurricane Sally, field and reanalysis data from various sources were obtained. Standard meteorological data from two NOAA National Data Buoy Center (NDBC) stations were used (Fig. 1): buoy station 42012 offshore of Orange Beach, Alabama (ORB), and DPIA1 (DI) on Dauphin Island, Alabama. The meteorological data included air temperature, relative humidity/dewpoint temperature (ORB only), and wind speed and direction. These stations were the closest measurements available to the main mooring site (CP). In addition, incoming solar radiation and relative humidity/dewpoint temperature data from the Dauphin Island station of the Alabama Real-Time Coastal Observing System (ARCOS) were obtained. This site is less than 500 m away from DPIA1, and both sites are collectively referred to as site DI for this study (Fig. 1). Additional data for key atmospheric variables, including outgoing solar radiation and longwave radiation, were obtained from the NCEP North American Region Reanalysis (NARR) for the grid cell closest to sites DI and ORB. A comparison between the incoming solar radiation data at site DI and the NARR reanalysis output at site DI and site ORB was conducted (Fig. S2a in the online supplemental material). While generally similar, there were some differences, and the observed data at DI were assumed to be most representative for the region. Existing methods were used to determine estimates for surface heat flux terms (e.g., Fairall et al. 1996) and the associated temperature tendency budget (e.g., Moisan and Niiler 1998). For the latent and sensible heat flux components, the methods of Fairall et al. (1996) produced transfer coefficients for temperature (i.e., Stanton number) and moisture (i.e., Dalton number) in the range of 1.0×10^{-3}–1.3×10^{-3}. These values are consistent with the 1.16×10^{-3} and 1.3×10^{-3} used in other studies (e.g., Huang et al. 2009; Potter et al. 2017). Hydrographic and current velocity data were obtained from a long-term mooring station (site CP) on the 20-m isobath to the west-southwest of Mobile Bay (Fig. 1). Site CP consisted of two CTD instruments that measured temperature and salinity at the bottom and near-surface, six thermistors throughout the water column that measured thermal structure and a 600-kHz Nortek Acoustic Doppler Waves and Current (AWAC) profiler that measured current velocity data throughout the water column. In addition to this site, three other monitoring stations collected data during the passage of Hurricane Sally: sites DI, ORB, and Perdido Pass (PP) in Fig. 1. Site ORB provided near-surface water temperature at ~2 m below the surface. Site PP provided near-bottom (~0.5 m above the bottom) hydrographic data in ~3 m of water at the mouth of Perdido Bay, similar to site DI. A calibration error was identified in the raw temperature data at site DI and was corrected by 1°C (Fig. S1 in the online supplemental material); the offset was identified during the instrument swap on 28 August.

These four stations were grouped into coastal sites with typical water column depths of ~3 m (DI and PP) and shelf sites with depths of 20 and 25.9 m (CP and ORB, respectively). Data from site CP (Fig. 3a, along with Fig. S2b in the online supplemental material) showed that the inner/midshelf conditions were uniform for several days prior to the arrival of Hurricane Sally, suggesting that the hydrographic conditions at other monitoring sites were similarly homogeneous and the associated temperature data during the time between 13 September and landfall (0400 CST 16 September) can be considered as depth-average values. Thus, the observed temperature changes at the sites with point measurements of water temperature (either near the surface at site ORB or near the bottom at sites PP and DI) were interpreted as changes in the depth-average temperature at these stations (i.e., $T_{\text{observed}} = T_{\text{depth\_average}}$). In addition to the depth-average temperature, the tropical cyclone heat potential (TCHP) could be directly derived from temperature data through the water at site CP. Tropical cyclone heat potential is defined as $\text{TCHP} = \rho_o C_p \int_{z(26^\circ\text{C})}^{0} T(z) - 26^\circ\text{C}\, dz$, where ρ_o is seawater density ($\sim 1 \times 10^3$ kg m^{-3}), C_p is the heat capacity of seawater ($\sim 4 \times 10^3$ J kg^{-1} °C^{-1}), $T(z)$ is the vertical temperature structure, and $z(26^\circ\text{C})$ is the depth of the 26°C isotherm (Leipper and Volgenau 1972). Over shelf regions, this integration is often limited by the depth of the water column rather than the depth of the 26°C isotherm as is the case in this study. Thus, at site CP the integration in TCHP calculation is from the surface to the bottom. Relative water levels at sites DI and PP were determined by subtracting the broader study period mean [13 August–20 September from Dzwonkowski et al. (2021)] from site DI and adjusting site PP to match the de-meaned prestorm conditions at site DI.

c. *Satellite-derived sea surface temperature data*

Sea surface temperature data were obtained from the Jet Propulsion Laboratory (JPL) Multiscale Ultrahigh Resolution (MUR) sea surface temperature product (https://podaac.jpl.nasa.gov/dataset/MUR-JPL-L4-GLOB-v4.1). This is a daily 1-km-resolution product that blends 1-km infrared sensor data and 25-km microwave sensor data. Although this product is gap free, it is expected that the extensive cloud cover during the shelf crossing of Hurricane Sally severely limited the contribution of high-resolution data to this data product over the study period, likely limiting the quality of the data near the coastline. In addition, the daily resolution is expected to undersample the evolution of the temperature structure during shelf crossing of Hurricane Sally, which occurred over a period on the order of a day. Despite these limitations, the MUR sea surface temperature data compared reasonably well to the in situ data at the shelf sites (CP and ORB) over the month period surrounding the storm event (Figs. S3a,b in the online supplemental material). The root-mean-square error (rmse) was 0.41 and 0.33 and the r^2 was 0.93 and 0.81 for sites CP and ORB, respectively. Importantly, the conditions

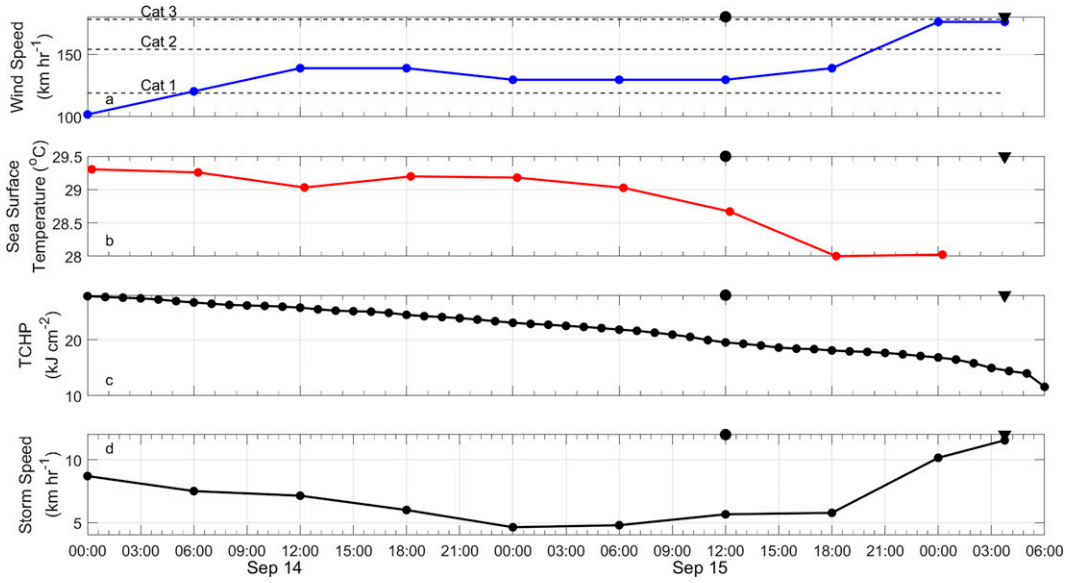

FIG. 2. Time series of (a) the maximum wind speed of Hurricane Sally, (b) the average sea surface temperature from the inner core using the MUR sea surface temperature product, (c) TCHP (see section 2b) at site CP, and (d) the translational speed of Hurricane Sally. In (a), Saffir–Simpson wind speeds for storm categories 1–3 (labels Cat 1–3) are indicated by the horizontal black dashed lines. The times at which the center of the storm reached the shelf break (filled circles) and made landfall (filled upside-down triangles) are marked on the top edge of the plots.

prior to the storm event as well as the temperature decrease during the passage of Hurricane Sally were generally similar. As such, the MUR sea surface temperature data were used to provide a broad regional picture of the conditions during the period of interest as well as a first-order estimate of the shelf thermal changes in response to Hurricane Sally. The surface temperature of the inner core of Hurricane Sally was determined using the values within the radius of maximum wind at the 6-h intervals of the best-track storm data on a given day.

3. Results

a. *Evolution of Hurricane Sally*

Hurricane Sally experienced two periods of rapid intensification. The first occurred over the deep Gulf of Mexico outside the study region early on 14 September (Figs. 1b and 2a). As the day progressed the storm began to interact with the shelf more directly as the radius of maximum wind neared the shelf break. Wind speed at the monitoring stations notably increased from 6–12 m s^{-1} on 13 September to 12–17 m s^{-1} on 14 September (Figs. 1a,b).

Despite the storm moving very slowly (Fig. 2d: 5–9 km h^{-1}), the sea surface temperature conditions in the inner core of the storm remained favorable for intensification with values ~29.3°C (Fig. 2b) and the storm intensity was generally steady during the following 24 h. As the storm continued to approach the shelf, the heat content at site CP, as represented by the TCHP, was ~25 kJ cm^{-2} and decreased over the course of the storm event (Fig. 2c). This value is well below the 60 kJ cm^{-2} typically associated with intensification in the open ocean (Mainelli et al. 2008).

Despite the low level of TCHP, storm intensification resumed on 15 September as the center of the storm crossed the shelf break, increasing from 130 km h^{-1} at 1200 CST to 176 km h^{-1} at 0000 CST the next day. This period of rapid intensification began at a time when shelf temperatures were decreasing with both satellite-derived inner core temperatures and in situ shelf temperatures dropping below 28.5°C (Figs. 2b and 3a), a value that has been statistically associated with rapid intensification (Kaplan and DeMaria 2003). However, the thermal conditions generally stayed around 28°C over the shelf until landfall. Here again, the translational speed of the storm from the shelf break to landfall was relatively slow, only exceeding 10 km h^{-1} in the hours just before landfall (Fig. 2d).

Aspects of the storm structure during the period of rapid intensification can be seen in the best-track data and NAM model outputs (Fig. 3). The central pressure of Hurricane Sally dropped throughout 15 September going from 982 hPa over the open Gulf of Mexico to 967 hPa prior to landfall (reaching 965 hPa at landfall). There was a clear strengthening in the wind speeds that accompanied this drop in central pressure as the storm crossed the shelf. Despite the drop in central pressure, the radius of maximum wind remained generally constant while crossing the shelf. There was a small reduction from 46 to 37 km as Hurricane Sally crossed the shelf break between 0600 and 1200 CST. While the radius of maximum wind was constant through the period of rapid intensification, Hurricane Sally became more symmetrical. The best-track data indicated that the 50-kt wind radius for the four quadrants of the tropical cyclone changed from 130, 74, 0, and 74 km (northeast, southeast, southwest, and northwest

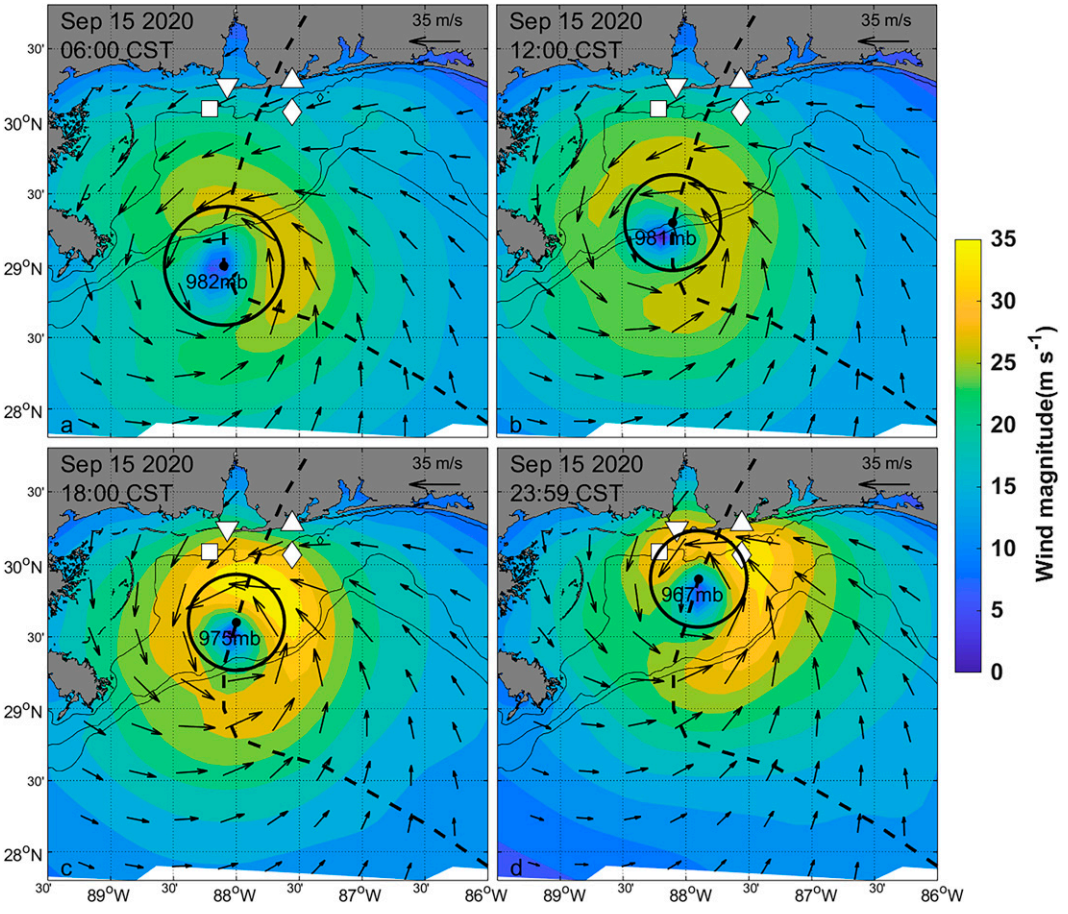

FIG. 3. A map of the Mississippi Bight showing the structural change/evolution of Hurricane Sally during intensification on 15 Sep at (a) 0600, (b) 1200, (c) 1800, and (d) 2359 CST. The wind conditions (black arrows and color shading) from the NAM model outputs as well as locations of the storm center (black dot), radius of maximum wind (black-outlined circle), and central pressure (black text within the radius of maximum wind) from the best-track data are provided in each panel. In addition, the full storm track is shown as a black dashed line and the monitoring stations are shown with symbols (DI: upside-down triangle, ORB: diamond, CP: square, and PP: triangle). Note that the wind vectors are at a reduced spatial resolution for visual clarity.

quadrants, respectively) at 1200 CST 15 September at the start of rapid intensification to 130, 74, 30, and 93 km on 2359 CST 15 September at the end of that period.

b. Evolution of sea surface temperature

Given the known importance of ocean temperature on storm intensity, the evolution of the shelf sea surface temperature conditions provided an important context for the observed air–sea interaction during the transit of Hurricane Sally over the shelf (Fig. 1). Prior to the arrival of Hurricane Sally in the Mississippi Bight (13 September), the sea surface temperature conditions were generally ~29.3°C with pockets of slightly warmer and cooler water throughout the region. These small deviations became enhanced as the storm approached the shelf on 14 September (Fig. 1b). There was notable cooling to the northeast of the storm track over the deep Gulf of Mexico that extended onto the shelf break. Even with this development of heterogeneity in the sea surface temperatures, the shelf was still generally above 28.5°C, consistent with an analysis of prestorm thermal conditions by Dzwonkowski et al. (2021) that estimated the foot of a downwelling front (using 28.5°C isotherm) to have crossed much of the shelf (Fig. 1b: gray dashed line) as well as consistent with the analysis of modeling outputs in Gramer et al. (2022). As the storm transited to the shelf on 15 September, the sea surface temperature cooling broadened across the region with maximum decreases generally directly under and to the left of the storm track. Nonetheless, a triangular patch of water with sea surface temperature of ~28.5°C was maintained while the storm crossed the shelf. The shelf around the storm track was homogenously cooled to <28°C with the storm making landfall and tracking well inland of the coast on 16 September.

c. Thermal evolution of the shelf and coastal stations

A similar temperature evolution was observed in the monitoring stations (Fig. 4a). Consistent with the satellite-derived sea

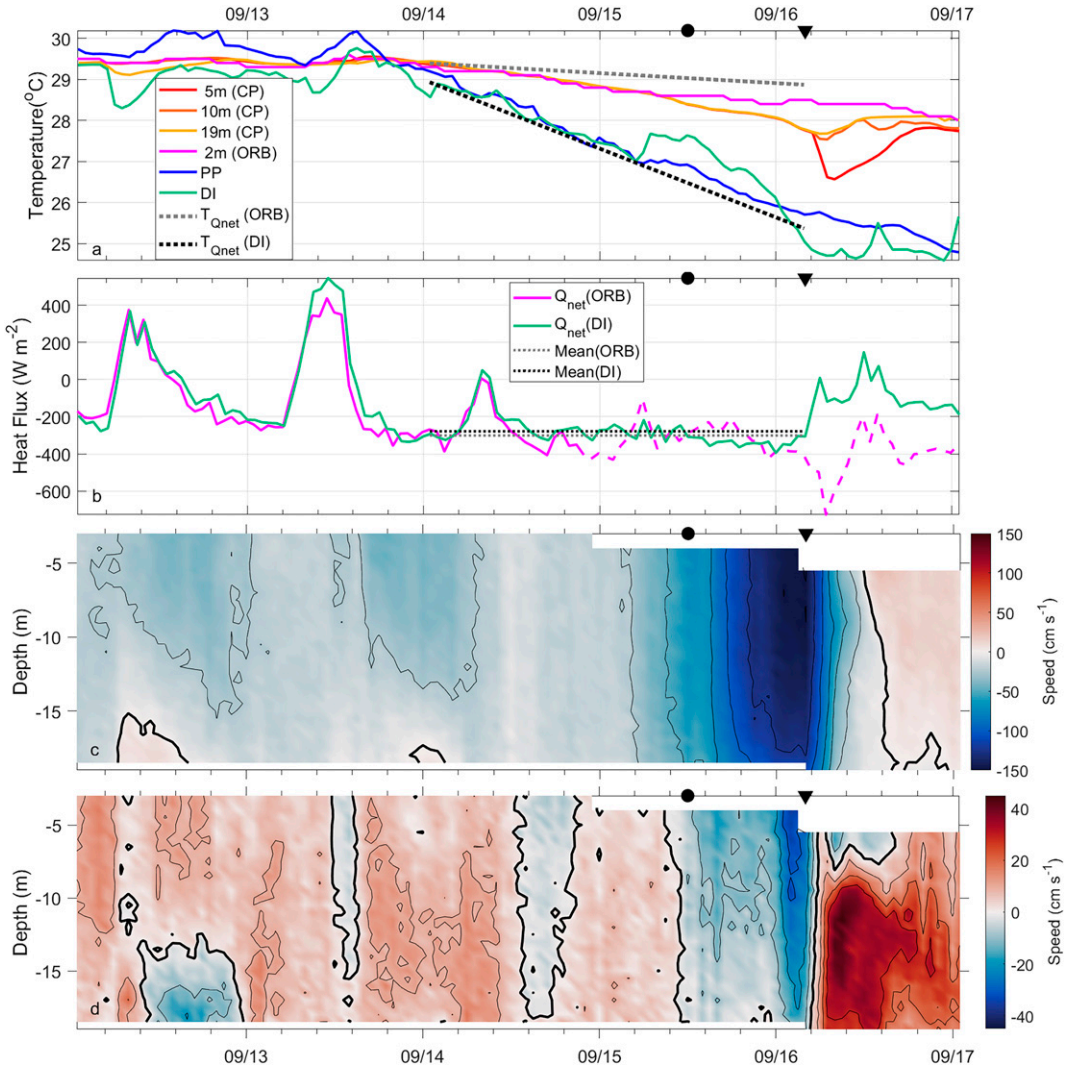

FIG. 4. Time series of (a) water temperature at the labeled monitoring sites, (b) surface heat flux Q_{net} at sites ORB and DI, (c) along-shelf currents at site CP, and (d) across-shelf currents at site CP. In (b), the dotted horizontal lines indicate the average surface heat flux from 14 Sep to landfall on 16 Sep at DI (larger black) and ORB (smaller gray). Note that the dashed line (magenta) in (b) indicates surface flux estimates at ORB using the relative humidity from DI. In (c) and (d), the black contours indicate velocity intervals of 25 and 10 cm s^{-1}, respectively, with the thick line being 0 cm s^{-1}. Eastward and northward currents are shown with positive values, and westward and southward currents are shown with negative values. The times at which the center of Hurricane Sally reached the shelfbreak (filled circles) and made landfall (filled upside-down triangles) are marked on the top edge of the plots. The color maps in (c) and (d) are from Thyng et al. (2016).

surface temperature, the in situ temperatures at the shelf stations were generally ~29.4°C on 13 September. The direct impact of Hurricane Sally on the coastal ocean became apparent on 14 September as the wind conditions increased (Figs. 1a,b) and the temperatures began a near simultaneous decrease. Both shelf sites (CP and ORB) had similar temperature tendencies through the first 1.5 days of this decline period (Fig. 4a). The temperature behavior at these two sites began to diverge ~16 h prior to landfall as Hurricane Sally moved northward over the shelf (1200 CST 15 September). At this point, the temperature decrease slowed at ORB and became warmer than that at site CP. By landfall, site ORB had cooled by ~0.9°C as compared with ~1.6°C at CP. This east–west temperature gradient, with relatively colder conditions to the left of the storm track, was consistent with the satellite-derived sea surface temperature data.

The temperature tendencies at the coastal stations experienced a clear separation from the shelf conditions with much faster cooling rates. As a result, coastal temperatures reached values of 25°–26°C prior to landfall. Similar to the shelf sites, there was a notable deviation in the cooling rates between sites just prior to landfall, with the rate at site DI (left of the

storm center) higher than that at site PP (right of the storm center). A comparison of the coastal and shelf stations showed that there was also a notable north–south gradient that was not captured in satellite-derived sea surface temperature data. Despite this nearshore limitation in the satellite-derived sea surface temperature data, the broader shelf patterns were consistent with in situ data at the shelf sites.

d. Heat budget analysis

To further investigate the thermal response of the coastal ocean during this cooling period between 14 and 16 September, simplified heat budgets for DI and ORB were estimated. The simplest heat budget for the temperature tendency in a well-mixed water column can be represented as

$$\frac{\partial \overline{T}}{\partial t} = \frac{Q_{\text{net}}}{\rho_o c_p h} = \frac{Q_{\text{sw}} + Q_b + Q_e + Q_h + Q_r}{\rho_o c_p h}, \qquad (1)$$

where $\overline{T}$ is the depth-average temperature, Q_{net} is the total surface heat flux, ρ_o is the depth-average density, c_p is the heat capacity of seawater, h is the water depth, Q_{sw} is the shortwave heat flux, Q_b is the net longwave heat flux, Q_e is the latent heat flux, Q_h is the sensible heat flux, and Q_r is the precipitation-induced heat flux. Huang et al. (2009) noted that the heat flux derived from hurricane-induced precipitation was negligible and was not considered, as has been done in other studies (e.g., Potter et al. 2017). The remaining heat flux terms (Fig. S2 in the online supplemental material) indicated that Q_e was the dominant term during this period with values typically ~250 W m^{-2}. Similarly, Q_{net} for both sites showed outward fluxes ~300 W m^{-2} (Fig. 4b).

To get a first-order estimate of the importance of the surface heat flux, Q_{net} averaged over this period was used to estimate the expected rate of temperature change solely from the surface heat flux. For site DI, a water depth of 3.5 m (i.e., mean site depth plus the average surge over the event period) and an average outward Q_{net} of 278 W m^{-2} (Fig. 4b: black dashed line) resulted in a temperature decrease of 0.070°C h^{-1}. This rate was then used to project the temperature change over the period of decline for the coastal stations (Fig. 4a: black dashed line). For site ORB, an estimate using a water depth of 25.9 m (i.e., mean depth) and an average outward Q_{net} of 301 W m^{-2} (Fig. 4b: gray dashed line) yielded a temperature decrease of 0.010°C h^{-1} from which the temperature change was also projected over this time period for the shelf sites (Fig. 4a: gray dashed line). In the case of the coastal stations, this surface flux-based temperature tendency was very close to the observed temperature tendency of ~0.071°C h^{-1} (i.e., ~3.7°C in 52 h) and generally well represented the coastal temperature decline. By comparison, the shelf stations' surface flux-based tendency had a larger difference, with the observed tendency being ~0.017°C h^{-1} (i.e., 0.9°C in 52 h), higher by a factor of ~1.7.

While Eq. (1) was surprisingly effective in capturing the order-of-magnitude change at both coastal and shelf stations, station to station changes in the temperature declines became increasingly apparent as the storm crossed the shelf. The stations westward (left) of the storm center decreased more rapidly than those eastward (right) suggesting coastal circulation may have had a significant role in the temperature budget. The arrangement of stations allow for a first-order estimate of the advective components at CP, that is $\overline{u}(\Delta\overline{T}_{\text{al}}/\Delta x)$ and $\overline{v}(\Delta\overline{T}_{\text{ac}}/\Delta y)$, where $\overline{u}$ is the depth-average along-shelf velocity, $\overline{v}$ is the depth-average across-shelf velocity, $\Delta\overline{T}_{\text{al}}$ is the along-shelf temperature difference between sites CP and ORB, $\Delta\overline{T}_{\text{ac}}$ is the across-shelf temperature difference between sites CP and DI, Δx is the distance between sites CP and ORB, and Δy is the distance between sites CP and DI. At the onset of the temperature decline, both terms were relatively small (Fig. 5a). The along-shelf advection had virtually no flux from 0100 CST 14 September to 1200 CST 15 September because of the lack of an along-shelf temperature gradient between CP and ORB (Fig. 4a). Over this period, the across-shelf advection term had a weak diurnal pattern associated with oscillatory currents that were modulated by a low-frequency onshore flow coincident with the rising on water level at the coast (Fig. 4d, along with Fig. S1c in the online supplemental material).

As the storm transited to the shelf (from 1200 CST 15 September to 0345 CST 16 September), the advection terms increased in magnitude in response to the cyclonic wind forcing (Fig. 4c). Very strong westward along-shelf flow amplified the small but growing temperature difference between CP and ORB and provided a positive heat flux to the site CP. In contrast, the strong across-shelf flow transported cooler, shallow water offshore driving a negative heat flux to site CP. The advection terms were very similar in magnitude during the majority of the shelf crossing, $O(10^{-5})$°C s^{-1}. However, in the hours before landfall, the magnitude of the across-shelf term increased faster than that of the along-shelf term, eventually exceeding the along-shelf values by more than double. The cumulative impact of these advective heat fluxes was the same order of magnitude, producing temperature changes of 0.4° and −0.7°C for the along-shelf and across-shelf contributions, respectively. These advective contributions to the temperature change at site CP and the changes driven by the surface fluxes calculated at ORB combined to result in a total temperature change of ~1.0°C (Fig. 5b, summing the cumulative temperature values at landfall, 0345 CST 16 September). While this value underrepresents the observed change at site CP ($\Delta T \sim 1.6$°C) by ~38%, the result still provides a rare observational, first-order perspective of the processes driving the temperature change at the site.

4. Discussion

a. Relative importance of surface fluxes

Upper-ocean cooling under tropical cyclones is typically associated with surface heat fluxes, vertical mixing, upwelling, and horizontal advection (Potter et al. 2017). Often entrainment of sub–mixed layer water is the dominant contributor to upper-ocean cooling (e.g., Price 1981; Ginis and Dikinov 1989; D'Asaro 2003; Price 2009). In contrast, the results of this work indicated surface heat fluxes were a dominating contributor in modifying the temperature conditions in the coastal zone. Focusing on the heat loss due to the enthalpy flux ($Q_{\text{enthalpy}} = Q_e + Q_h$), estimates of its relative importance

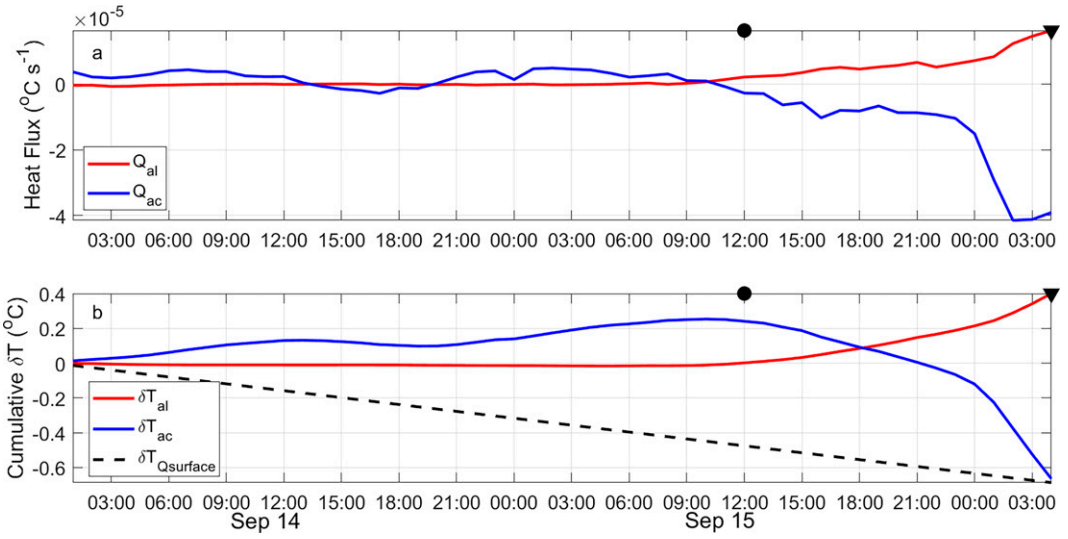

FIG. 5. Times series of thermal conditions, showing the (a) advective heat flux components and (b) cumulative contributions of the terms on the right-hand side of the simplified temperature budget for site CP [(Eq. (1)] during the period of decreasing temperature tendency prior to the landfall of Hurricane Sally (14–15 Sep), including the along- and across-shelf heat fluxes (δT_{al} and δT_{ac}, respectively) as well as the contribution from the temporal average surface heat flux derived at ORB ($\delta T_{Qsurface}$). The observed temperature change at the shelf sites over this time period was $O(1.6)$°C. The times at which the center of Hurricane Sally reached the shelf break (filled circles) and made land fall (filled upside-down triangles) are marked on the top edge of the plots.

could be obtained at two of the sites. At site ORB, the contribution of the $Q_{enthalpy}$ accounted for 0.53°C of the cooling over 14–16 September during the period prior to landfall. This amounts to ~59% of the total temperature change. The percent of cooling from $Q_{enthalpy}$ further increased moving shoreward, with nearly all of the cooling (~98%) at site DI accounted for by the sensible and latent heat fluxes.

This dominance of the $Q_{enthalpy}$ is notably different than what is typically seen in the open ocean. By comparison, studies in the open ocean have found the relative contribution of surface heat fluxes to be much lower. Potter et al. (2017) summarizes a number of open-ocean studies that found values of ~15%, while noting that D'Asaro (2003) found spatially varying contributions to the right (27%) and left (13%) of the storm center. In examining buoy data under four tropical cyclones, Potter et al. (2017) found that $Q_{enthalpy}$ had a much wider range of values than previously reported with contributions as high as 47%.

Nonetheless, these $Q_{enthalpy}$ contributions are lower than what was observed in this study. This is likely related to the well-mixed nature of the shelf prior to the arrival of Hurricane Sally. As mentioned, Dzwonkowski et al. (2021) estimated that more than half the shelf was vertically uniform prior to the arrival of Hurricane Sally. Thus, cooling from vertical entrainment was not possible. In addition, the velocity structure at site CP showed no across-shelf circulation patterns consistent with coastal upwelling as the flow was southward over the full extent of the water during the shelf transit of Hurricane Sally (Fig. 4d). Thus, both entrainment of submixed layer water as well as upwelling were not significant contributors to the inner/midshelf heat budget, allowing only surface fluxes and advection to dominate the changes in the temperature tendency.

b. *Assessing TCHP for storm intensification in the coastal zone*

In terms of the thermal capacity of the coastal ocean to support intensification, the shelf temperature remained above the 26°C (a value typically linked to sustained or intensifying storms) and was much closer to the 28.5°C [a threshold value statistically correlated with rapid intensification, per Kaplan and DeMaria (2003)]. Yet, the full water column data at site CP indicated that the TCHP was low (~15–20 kJ cm^{-2}), suggesting the shelf was a poor oceanic environment for intensification. As highlighted by Price (2009), this is in large part due to the shallow nature of continental shelves that limit the extent to which the heat content can be integrated above the 26°C isotherm (i.e., the bottom is reached well before the 26°C isotherm is reached). Even extrapolating the temperature conditions at site CP to a depth of 40 m, more than halfway across the shelf, the TCHP would still only be ~40 kJ cm^{-2}.

As has been suggested by previous studies (e.g., Price 2009; Potter et al. 2019), TCHP is not likely a good metric for determining the favorability of the coastal ocean for intensification. Rather, the depth-average water temperature may be a better metric for assessing coastal ocean conditions prior to and during the transit of tropical cyclones. This is consistent with the metric of depth-average temperature of the mixing depth that was suggested by Price (2009) and has been shown to be an effective predictor for tropical cyclone intensity in other open-

ocean studies (e.g., Lin et al. 2013; Balaguru et al. 2014; Balaguru et al. 2015).

c. *Shift in the region of maximum cooling*

While average sea surface temperatures under the inner core of Hurricane Sally were generally warm (Fig. 2b), the evolution of the shelf conditions presented complex patterns that have the potential to impact air–sea interactions prior to landfall. As highlighted by satellite-derived sea surface temperature data on 14–15 September, there was a growing east-to-west gradient with warm-to-cool thermal conditions where the storm transited to the shelf (Figs. 1b,c). The sea surface temperature structure was counter to the well-established rightward bias in cooling that is typically observed in the open ocean in the Northern Hemisphere (Price 1981; Stramma et al. 1986; D'Asaro et al. 2007; Sanabia and Jayne 2020; Zhang et al. 2021; Ma et al. 2021). This coastal transition to a leftward bias in the location of maximum cooling has been documented in a limited number of other studies on ocean–tropical cyclone interactions in the Bay of Bengal using largely modeling outputs and satellite-derived sea surface temperature data (Mahapatra et al. 2007; Das et al. 2017; Mandal et al. 2018; Chacko and Zimik 2018). However, to the authors' knowledge, this is the first study to provide in situ evidence of such behavior across the inner core of a storm.

Such a shift in thermal patterns may not be trivial as recent modeling studies on rapid intensification indicate the structuring of sea surface temperature gradients under a storm as well as inner core cooling as small as 0.3–0.4°C influenced storm intensity changes (Kanada et al. 2017; Zhang et al. 2020). In situ data used in this study indicate a surface water temperature difference of ~0.6°C across the radius of maximum wind at 0000 CST 16 September just prior to landfall. A first-order sense of the potential impact of this temperature gradient can be assessed by using the surface water temperature at site CP to compute a Q_{enthalpy} with the atmospheric conditions at ORB. The estimate was minimally different (~5%) from site ORB results when averaged over the whole period of the water temperature decline (0100 CST 14 September–0400 CST 16 September). However, focusing just on the period when the center of the storm was crossing the shelf (1200 CST 15 September–0400 CST 16 September), there was a larger difference in the Q_{enthalpy} with an ~18% smaller flux using surface water temperature at site CP. Interestingly, despite the notable spatial variability in the sea surface temperature field, the storm was able to rapidly intensify over the shelf. This may be because the initial conditions on the shelf were exceedingly warm (<28.5°C) so that, despite the growing spatial variability, shelf conditions remained largely above 28.0°C on 15 September (Fig. 1c) as did the average inner core sea surface temperature (Fig. 2b). This work suggests more research into the potential impacts of temperature gradients on tropical cyclones in coastal zones is needed.

d. *Role of shelf bathymetry for thermal structuring*

The processes driving this coastal response are, in part, directly related to the interplay of the storm forcing with coastal bathymetry (Fig. 6). At the onset of the shelf temperature decline on 14 September, differential cooling between the shallow coastal stations and deeper shelf stations played a critical role in generating an across-shelf temperature gradient as coastal and shelf sites with different depths had similar surface heat fluxes. Differences in the along-shelf temperature changes at the shelf stations became apparent over the course of 15–16 September (Fig. 4a), when the cyclonic rotation in the wind field became more intensified with rapidly increasing east-to-southeast wind at site ORB and an increasing north wind at site DI (Figs. 1c,d and 3). Given that the inner core of the storm moved across the shelf faster than the time scale for geostrophic adjustment (i.e., ~16 h to cross the shelf as compared with an ~24-h inertial time scale), the coastal circulation would be expected to follow the wind forcing with northward flow at site ORB and southward flow at site CP based on previous studies of coastal responses to storms (e.g., Keen and Glenn 1999; Mahapatra et al. 2007).

Such circulation patterns were consistent with the temperature tendency at sites CP and ORB as well as the velocity structure at site CP (Fig. 4). Onshore transport of deeper warmer water on the eastern side of the storm would be expected to slow the cooling rate as observed at site ORB, while offshore transport of cooler, shallower water on the western side of the storm would be expected to increase the rate of temperature decline as observed at site CP. Incredibly, site ORB experienced almost no cooling in the final hours before landfall despite encountering peak storm conditions as the eyewall passed over this region. This is consistent with the advection of warm offshore and/or eastward water arresting the cooling to the east of the storm center and limiting the ahead-of-eye cooling. Thus, the interaction between the depth-dependent thermodynamics of the water column and the storm-driven coastal circulation contributed to the observed temperature dipole across the shelf.

5. Conclusions

Although the duration of time that tropical cyclones spend over shelf regions of the ocean is typically short relative to their overall life span, significant changes in the storm characteristics can occur. The results of this study highlight the complex interactions between the storm forcing (e.g., track and intensity) and the coastal environment (e.g., initial hydrographic conditions and system bathymetry). Importantly, these coastal ocean–storm interactions over the shelf may be very different than those in the open ocean. This case study of Hurricane Sally highlights several such differences. In contrast to typical open-ocean responses in which maximum cooling occurs on the right side of storms in the Northern Hemisphere, the coastal response of Hurricane Sally demonstrated a leftward bias in the Mississippi Bight. Such horizontal spatial structure across the inner core of a tropical cyclone could impact the dynamic processes driving rapid intensification. A better understanding of the frequency of the observed spatial features as well as their potential importance requires further research but is critical for accurate storm forecasting. Given that in situ data on coastal water column structure during storm events are

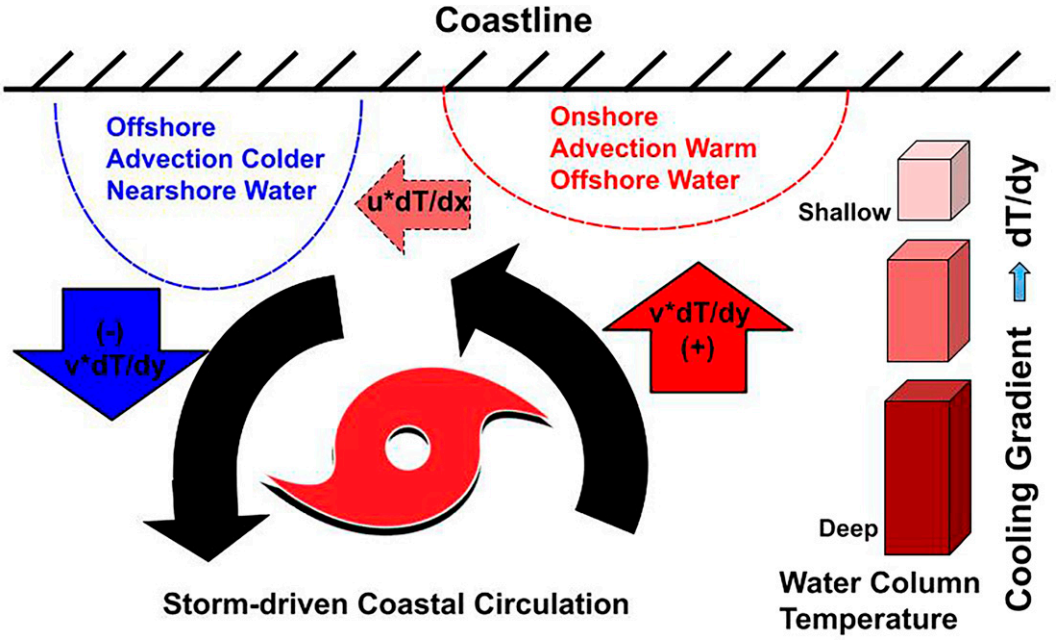

FIG. 6. Conceptual diagram showing a coastal ocean response pattern to an approaching tropical cyclone under well-mixed shelf conditions. The water column (red cubes) cools more rapidly in the nearshore water relative to the deeper shelf given that the water temperature change is inversely related to depth. The resulting temperature gradient leads to an onshore transport of warmer water on the right-hand side and an offshore transport of cooler water in a counterclockwise manner consistent with the primary wind circulation of the tropical cyclone (black arrows) in the Northern Hemisphere. As a result, the advection of heat (red and blue arrows) limits the water column heat loss on the right side of the storm and generates an expanding region of maximum cooling to the left of the storm. This leads to fine-scale changes in the sea surface temperature across the inner core of the storm prior to landfall.

likely to remain sparse, improving the understanding of the available satellite-derived sea surface temperature patterns may be useful for forecasting shelf intensification of tropical cyclones.

More important, this event exhibited characteristics that typically limit the potential for intensification in the open ocean. First, the shallow nature of the shelf environment constrained the magnitude of the TCHP, $O(20–40)$ kJ cm^{-2}, generally below the value of 60 kJ cm^{-2} typically associated with intensification in the open ocean (Mainelli et al. 2008). These observations are consistent with the growing body of literature that highlights the fact that TCHP does not properly represent the role that shelf conditions exert on storm strength (e.g., Price 2009; Potter et al. 2019). Second, Hurricane Sally had a slow translational speed as it crossed the shelf. Slow-moving storms in the open ocean are typically associated with attenuation due to cooler sea surface temperatures driven by mixing and upwelling from prolonged exposure to storm conditions (e.g., Price 1981; Lloyd and Vecchi 2011; Vincent et al. 2012; Walker et al. 2014; Zhang et al. 2016; Park et al. 2019). By contrast, the warm vertically homogenous state of the coastal ocean prior to the arrival of the storm inner core (i.e., the clearing of cooler bottom water from the shelf) eliminated this self-damping process associated with slower open-ocean tropical cyclones. Despite this coupling of "weak" thermal potential in the coastal ocean state and slow translational speed, Hurricane Sally was able to rapidly intensify over the shelf defying the conventional open-ocean expectations. Such unexpected behavior of Hurricane Sally demonstrates the critical need to better understand the importance of initial shelf setup and the direct air–sea interactions that regulate the feedbacks between the coastal ocean and tropical cyclone intensity.

It is important to note that the ocean state is only one component that contributes to tropical cyclone strength. A fuller understanding the processes driving rapid intensification over the coastal ocean requires additional consideration of ambient atmospheric conditions (e.g., vertical wind shear, dry air entrainment) and internal storm dynamics (e.g., changes in storm size and the associated acceleration from the conservation of angular momentum) and how these change as the system interacts with the terrestrial environment. Without a better understanding of the processes that determine the onset and evolution of rapid intensification of tropical cyclones in coastal settings, society's ability to develop the necessary resiliency to such events in a changing climate will be inadequate.

Acknowledgments. This work would not have been possible without the many folks that have passed through the Tech Support Group at the Dauphin Island Sea Lab to help to maintain site CP over the years. We thank Rich Pawlowicz at the University of British Columbia for the freely available

MATLAB m_map toolbox and Chris Landsea of NOAA NHC for providing links to early versions of the NOAA NHC ATCF best-track data for 2020 storms. A portion of this work was conducted at the Jet Propulsion Laboratory, California Institute of Technology, under contract with NASA. This research was made possible by the NOAA RESTORE Science Program (NA17NOS4510101 and NA19NOS4510194) and the NASA Physical Oceanography program (80NSSC21K0553 and WBS 281945.02.25.04.67) and NOAA IOOS program via GCOOS (NA16NOS0120018). The authors declare that they have no competing interests.

Data availability statement. All data that were not downloaded from public sources have been made publicly available through the Dauphin Island Data Management Center (https://www.disl.edu/research/data-management-center) and the NOAA National Centers for Environmental Information (NCEI). In particular, site CP data are available at the following links: https://accession.nodc.noaa.gov/0211052; https://www.ncei.noaa.gov/access/metadata/landing-page/bin/iso?id=gov.noaa.nodc:0241013; https://doi.org/10.25921/a4vk-ts66; https://doi.org/10.25921/h08h-xk81; https://doi.org/10.25921/5za5-aw02; https://doi.org/10.25921/gaj9-tp70; https://doi.org/10.25921/yy2w-ad34; https://data.nodc.noaa.gov/cgi-bin/iso?id=gov.noaa.nodc:0203749; https://doi.org/10.25921/gnd8-5h49; https://doi.org/10.25921/4qqm-3332; and https://doi.org/10.25921/q1tz-3b62.

REFERENCES

Balaguru, K., S. Taraphdar, L. Leung, and G. Foltz, 2014: Increase in the intensity of postmonsoon Bay of Bengal tropical cyclones. *Geophys. Res. Lett.*, **41**, 3594–3601, https://doi.org/10.1002/2014GL060197.

——, G. Foltz, L. Leung, D. Asaro, K. Emanuel, H. Liu, and S. Zedler, 2015: Dynamic potential intensity: An improved representation of the Ocean's impact on tropical cyclones. *Geophys. Res. Lett.*, **42**, 6739–6746, https://doi.org/10.1002/2015GL064822.

Berg, R., and B. J. Reinhart, 2021: National Hurricane center tropical cyclone report: Hurricane Sally (AL192020). NHC Tech. Rep., 69 pp., https://www.nhc.noaa.gov/data/tcr/AL192020_Sally.pdf.

Bhatia, K. T., G. A. Vecchi, T. R. Knutson, H. Murakami, J. Kossin, K. W. Dixon, and C. E. Whitlock, 2019: Recent increases in tropical cyclone intensification rates. *Nat. Commun.*, **10**, 3942, https://doi.org/10.1038/s41467-019-11922-2.

Chacko, N., and L. Zimik, 2018: Effect of Cyclone Thane in the Bay of Bengal explored using moored buoy observations and multi-platform satellite data. *Photonirvachak*, **46**, 821–828, https://doi.org/10.1007/s12524-017-0748-9.

Cheriton, O. M., C. D. Storlazzi, K. J. Rosenberger, C. E. Sherman, and W. E. Schmidt, 2021: Rapid observations of ocean dynamics and stratification along a steep island coast during Hurricane María. *Sci. Adv.*, **7**, eabf1552, https://doi.org/10.1126/sciadv.abf1552.

Chu, J. E., S. S. Lee, A. Timmermann, C. Wengel, M. F. Stuecker, and R. Yamaguchi, 2020: Reduced tropical cyclone densities and ocean effects due to anthropogenic greenhouse warming. *Sci. Adv.*, **6**, eabd5109, https://doi.org/10.1126/sciadv.abd5109.

Das, Y., U. C. Mohanty, and I. Jain, 2017: Numerical simulation on Bay of Bengal's response to cyclones using the Princeton ocean model. *Braz. J. Oceanogr.*, **65**, 128–145, https://doi.org/10.1590/s1679-87592017111206502.

D'Asaro, E. A., 2003: The ocean boundary layer below Hurricane Dennis. *J. Phys. Oceanogr.*, **33**, 561–579, https://doi.org/10.1175/1520-0485(2003)033<0561:TOBLBH>2.0.CO;2.

——, T. B. Sanford, P. P. Niiler, and E. J. Terrill, 2007: Cold wake of hurricane Frances. *Geophys. Res. Lett.*, **34**, L15609, https://doi.org/10.1029/2007GL030160.

DeMaria, M., C. R. Sampson, J. A. Knaff, and K. D. Musgrave, 2014: Is tropical cyclone intensity guidance improving? *Bull. Amer. Meteor. Soc.*, **95**, 387–398, https://doi.org/10.1175/BAMS-D-12-00240.1.

Dzwonkowski, B., S. Fournier, K. Park, S. L. Dykstra, and J. T. Reager, 2018: Water column stability and the role of velocity shear on a seasonally stratified shelf, Mississippi Bight, Northern Gulf of Mexico. *J. Geophys. Res. Oceans*, **123**, 5777–5796, https://doi.org/10.1029/2017JC013624.

——, J. Coogan, S. Fournier, G. Lockridge, K. Park, and T. Lee, 2020: Compounding impact of severe weather events fuels marine heatwave in the coastal ocean. *Nat. Commun.*, **11**, 4623, https://doi.org/10.1038/s41467-020-18339-2.

——, S. Fournier, G. Lockridge, J. Coogan, Z. Liu, and K. Park 2021: Cascading weather events amplify the coastal thermal conditions prior to the shelf transit of Hurricane Sally (2020). *J. Geophys. Res. Oceans*, **126**, e2021JC017957, https://doi.org/10.1029/2021JC017957.

Emanuel, K., 2017: Will global warming make hurricane forecasting more difficult? *Bull. Amer. Meteor. Soc.*, **98**, 495–501, https://doi.org/10.1175/BAMS-D-16-0134.1.

Fairall, C. W., E. F. Bradley, D. P. Rogers, J. B. Edson, and G. S. Young, 1996: Bulk parameterization of air-sea fluxes for tropical ocean-global atmosphere coupled-ocean atmosphere response experiment. *J. Geophys. Res.*, **101**, 3747–3764, https://doi.org/10.1029/95JC03205.

Freeman, P., and K. Warner, 2001: Vulnerability of infrastructure to climate variability: How does this affect infrastructure lending policies? World Bank Rep., 42 pp.

Garzon, J. L., C. M. Ferreira, and R. Padilla-Hernandez, 2018: Evaluation of weather forecast systems for storm surge modeling in the Chesapeake Bay. *Ocean Dyn.*, **68**, 91–107, https://doi.org/10.1007/s10236-017-1120-x.

Ginis, I., and K. Z. Dikinov, 1989: Modeling of the Typhoon Virginia (1978) forcing on the ocean. *Sov. Meteor. Hydrol. Engl. Transl.*, **7**, 53–60.

Gramer, L. J., J. Zhang, G. Alaka, A. Hazelton, and S. Gopalakrishnan, 2022: Coastal downwelling intensifies landfalling hurricanes. *Geophys. Res. Lett.*, **49**, e2021GL096630, https://doi.org/10.1029/2021GL096630.

Huang, P., T. Sanford, and J. Imberger, 2009: Heat and turbulent kinetic energy budgets for surface layer cooling induced by the passage of Hurricane Frances (2004). *J. Geophys. Res.*, **114**, C12023, https://doi.org/10.1029/2009JC005603.

Kanada, S., S. Tsujino, H. Aiki, M. K. Yoshioka, Y. Miyazawa, K. Tsuboki, and I. Takayabu, 2017: Impacts of SST patterns on rapid intensification of Typhoon Megi (2010). *J. Geophys. Res. Atmos.*, **122**, 13 245–13 262, https://doi.org/10.1002/2017JD027252.

Kaplan, J., and M. DeMaria, 2003: Large-scale characteristics of rapidly intensifying tropical cyclones in the North Atlantic basin. *Wea. Forecasting*, **18**, 1093–1108, https://doi.org/10.1175/1520-0434(2003)018<1093:LCORIT>2.0.CO;2.

——, ——, and J. A. Knaff, 2010: A revised tropical cyclone rapid intensification index for the Atlantic and eastern North Pacific basins. *Wea. Forecasting*, **25**, 220–241, https://doi.org/10.1175/2009WAF2222280.1.

Keen, T. R., and S. M. Glenn, 1999: Shallow water currents during Hurricane Andrew. *J. Geophys. Res.*, **104**, 23 443–23 458, https://doi.org/10.1029/1999JC900180.

Lee, C. Y., M. K. Tippett, A. H. Sobel, and S. J. Camargo, 2016: Rapid intensification and the bimodal distribution of tropical cyclone intensity. *Nat. Commun.*, **7**, 10625, https://doi.org/10.1038/ncomms10625.

Leipper, D., and D. Volgenau, 1972: Upper ocean heat content of the Gulf of Mexico. *J. Phys. Oceanogr.*, **2**, 218–224, https://doi.org/10.1175/1520-0485(1972)002<0218:HHPOTG>2.0.CO;2.

Lin, I. I., and Coauthors, 2013: An ocean coupling potential intensity index for tropical cyclones. *Geophys. Res. Lett.*, **40**, 1878–1882, https://doi.org/10.1002/grl.50091.

Liu, Z., H. Wang, Y. Zhang, L. Magnusson, J. Loftis, and D. Forrest, 2020: Cross-scale modeling of storm surge, tide, and inundation in Mid-Atlantic Bight and New York City during Hurricane Sandy, 2012. *Estuarine Coastal Shelf Sci.*, **233**, 106544, https://doi.org/10.1016/j.ecss.2019.106544.

Lloyd, I. D., and G. A. Vecchi, 2011: Observational evidence for oceanic controls on hurricane intensity. *J. Climate*, **24**, 1138–1153, https://doi.org/10.1175/2010JCLI3763.1.

Ma, Z., Y. Zhang, R. Wu, and R. Na, 2021: Statistical characteristics of the response of sea surface temperatures to westward typhoons in the South China Sea. *Remote Sens.*, **13**, 916, https://doi.org/10.3390/rs13050916.

Mahapatra, D. K., A. D. Rao, S. V. Babu, and C. Srinivas, 2007: Influence of coastline on upper Ocean's response to the tropical cyclone. *Geophys. Res. Lett.*, **34**, L17603, https://doi.org/10.1029/2007GL030410.

Mainelli, M., M. DeMaria, L. K. Shay, and G. Goni, 2008: Application of oceanic heat content estimation to operational forecasting of recent Atlantic category 5 hurricanes. *Wea. Forecasting*, **23**, 3–16, https://doi.org/10.1175/2007WAF2006111.1.

Mandal, S., S. Sil, A. Shee, and R. Venkatesan, 2018: Upper ocean and subsurface variability in the Bay of Bengal during Cyclone Roanu: A synergistic view using in situ and satellite observations. *Pure Appl. Geophys.*, **175**, 4605–4624, https://doi.org/10.1007/s00024-018-1932-8.

Miyamoto, Y., and T. Takemi, 2010: An effective radius of the sea surface enthalpy flux for the maintenance of a tropical cyclone. *Atmos. Sci. Lett.*, **11**, 278–282, https://doi.org/10.1002/asl.292.

Moisan, J. R., and P. P. Niiler, 1998: The seasonal heat budget of the North Pacific: Net heat flux and heat storage rates (1950–1990). *J. Phys. Oceanogr.*, **28**, 401–421, https://doi.org/10.1175/1520-0485(1998)028<0401:TSHBOT>2.0.CO;2.

Park, J.-H., and Coauthors, 2019: Rapid decay of slowly moving Typhoon Soulik (2018) due to interactions with the strongly stratified northern East China Sea. *Geophys. Res. Lett.*, **46**, 14 595–14 603, https://doi.org/10.1029/2019GL086274.

Potter, H., W. Drennan, and H. Graber, 2017: Upper ocean cooling and air-sea fluxes under typhoons: A case study. *J. Geophys. Res. Oceans*, **122**, 7237–7252, https://doi.org/10.1002/2017JC012954.

——, S. F. DiMarco, and A. H. Knapp, 2019: Tropical cyclone heat potential and the rapid intensification of Hurricane Harvey in the Texas bight. *J. Geophys. Res. Oceans*, **124**, 2440–2451, https://doi.org/10.1029/2018JC014776.

Price, J. F., 1981: Upper ocean response to a hurricane. *J. Phys. Oceanogr.*, **11**, 153–175, https://doi.org/10.1175/1520-0485(1981)011<0153:UORTAH>2.0.CO;2.

——, 2009: Metrics of hurricane-ocean interaction: Vertically-integrated or vertically-averaged ocean temperature? *Ocean Sci.*, **5**, 351–368, https://doi.org/10.5194/os-5-351-2009.

Pun, I.-F., and Coauthors, 2019: Rapid intensification of Typhoon Hato (2017) over shallow water. *Sustainability*, **11**, 3709, https://doi.org/10.3390/su11133709.

Sanabia, E. R., and S. R. Jayne, 2020: Ocean observations under two major hurricanes: Evolution of the response across the storm wakes. *AGU Adv.*, **1**, e2019AV000161, https://doi.org/10.1029/2019AV000161.

Seroka, G., T. Miles, Y. Xu, J. Kohut, O. Schofield, and S. Glenn, 2016: Hurricane Irene sensitivity to stratified coastal Ocean cooling. *Mon. Wea. Rev.*, **144**, 3507–3530, https://doi.org/10.1175/MWR-D-15-0452.1.

——, ——, ——, ——, ——, and ——, 2017: Rapid shelf-wide cooling response of a stratified coastal ocean to hurricanes. *J. Geophys. Res. Oceans*, **122**, 4845–4867, https://doi.org/10.1002/2017JC012756.

Stramma, L., P. Cornillon, and J. F. Price, 1986: Satellite observations of sea surface cooling by hurricanes. *J. Geophys. Res.*, **91**, 5031–5035, https://doi.org/10.1029/JC091iC04p05031.

Thyng, K. M., C. A. Greene, R. D. Hetland, H. M. Zimmerle, and S. F. DiMarco, 2016: True colors of oceanography: Guidelines for effective and accurate colormap selection. *Oceanography*, **29**, 9–13, https://doi.org/10.5670/oceanog.2016.66.

Vincent, E. M., M. Lengaigne, J. Vialard, G. Madec, N. C. Jourdain, and S. Masson, 2012: Assessing the oceanic control on the amplitude of sea surface cooling induced by tropical cyclones. *J. Geophys. Res.*, **117**, C05023, https://doi.org/10.1029/2011JC007705.

Walker, N. D., R. R. Leben, C. T. Pilley, M. Shannon, D. C. Herndon, I.-F. Pun, I.-I. Lin, and C. L. Gentemann, 2014: Slow translation speed causes rapid collapse of northeast Pacific Hurricane Kenneth over cold core eddy. *Geophys. Res. Lett.*, **41**, 7595–7601, https://doi.org/10.1002/2014GL061584.

Zhai, A. R., and J. H. Jiang, 2014: Dependence of US hurricane economic loss on maximum wind speed and storm size. *Environ. Res. Lett.*, **9**, 064019, https://doi.org/10.1088/1748-9326/9/6/064019.

Zhang, H., D. Chen, L. Zhou, X. Liu, T. Ding, and B. Zhou, 2016: Upper ocean response to Typhoon Kalmaegi (2014). *J. Geophys. Res. Oceans*, **121**, 6520–6535, https://doi.org/10.1002/2016JC012064.

——, H. He, W. Z. Zhang, and D. Tian, 2021: Upper ocean response to tropical cyclones: A review. *Geosci. Lett.*, **8**, 1, https://doi.org/10.1186/s40562-020-00170-8.

Zhang, Z., Y. Wang, W. Zhang, and J. Xu, 2019: Coastal ocean response and its feedback to Typhoon Hato (2017) over the South China Sea: A numerical study. *J. Geophys. Res. Atmos.*, **124**, 13 731–13 749, https://doi.org/10.1029/2019JD031377.

——, W. Zhang, W. Zhao, and C. Zhao, 2020: Radial distributions of sea surface temperature and their impacts on the rapid intensification of Typhoon Hato (2017). *Atmosphere*, **11**, 128, https://doi.org/10.3390/atmos11020128.